

RESEARCH ARTICLE

Open Access



Geophysical constraints on microbial biomass in subseafloor sediments and coal seams down to 2.5 km off Shimokita Peninsula, Japan

Wataru Tanikawa^{1,2*} , Osamu Tada³, Yuki Morono^{1,2}, Kai-Uwe Hinrichs⁴ and Fumio Inagaki^{1,2,5}

Abstract

To understand the ability of microbial life to inhabit a deep subseafloor coalbed sedimentary basin, the correlation between fluid transport properties and the abundance of microbial cells was investigated based on core samples collected down to about 2.5 km below the seafloor during the Integrated Ocean Drilling Program Expedition 337 off the Shimokita Peninsula, Japan. The overall depth profiles for porosity and permeability exhibited a decreasing trend with increasing depth. However, at depths greater than 1.2 km beneath the seafloor, the transport characteristics of the sediments were highly variable, with the permeability ranging from 10^{-16} to 10^{-22} m² and the pore size ranging from < 0.01 to 100 μ m. This is mainly attributed to the diversity of the lithology, which exhibits a range of pore sizes and pore geometries. Fracture channels in coal seams had the highest permeability, while shale deposits had the smallest pore size and lowest permeability. A positive correlation between permeability and pore size was confirmed by the Kozeny-Carman equation. Cell abundance at shallower depths was positively correlated with porosity and permeability, and was less strongly correlated with pore size. These findings suggest that one of the factors affecting the decrease in microbial cell abundance with increasing depth was a reduction in nutrient and water supply to indigenous microbial communities as a result of a decrease in porosity and permeability due to sediment compaction. Anomalous regions with relatively high cell concentrations in coal-bearing units could be explained by the higher permeability and larger pore size for these units compared to the surrounding sediments. Nutrient transport through permeable cleats in coal layers might occur upwards toward the upper permeable sandstone layers, which are well suited for sustaining sizable microbial populations. Conversely, impermeable shale and siltstone with small pores (< 0.2 μ m, which is smaller than microbial cell size) may act as barriers to water and energy-yielding substrates for deep microbial life. We propose that the pore size and permeability govern the threshold for microbial habitability in the deep subseafloor sedimentary biosphere.

Keywords: Deep biosphere, Lignite coal, Limits of life, Microbial community, Pore size, Porosity, Permeability, Habitability

Introduction

Previous scientific ocean drilling investigations have demonstrated that microbial communities are widespread in shallow and deep subseafloor sediments down to depths of 2.5 km below the ocean floor (Parkes et al. 1994; Lipp et al. 2008; Kallmeyer et al. 2012; Inagaki et al. 2015). These studies of sediment core samples generally showed

that microbial cell concentrations decrease logarithmically with increasing depth (Parkes et al. 1994; Lipp et al. 2008; Morono et al. 2009; Kallmeyer et al. 2012). The abundance and activity of microbial communities in deep subseafloor sediments depend on a variety of interrelated factors including the availability of water and nutrients (Abu-Ashour et al. 1994). The spatial variation in geological and geophysical conditions, such as temperature, pressure, pore water chemistry, pH, water activity (A_w), grain and pore geometries, and permeability, is manifested as spatiotemporal changes in microbial cell abundance, with in situ microbial population size and activity

* Correspondence: tanikawa@jamstec.go.jp

¹Kochi Institute for Core Sample Research, Japan Agency for Marine-Earth Science and Technology (JAMSTEC), Monobe B200, Nankoku, Kochi 783-8502, Japan

²Research and Development (R&D) Center for Submarine Resources, JAMSTEC, 2-15 Natsushima-cho, Yokosuka, Kanagawa 273-0061, Japan

Full list of author information is available at the end of the article

potentially affected by these conditions (Sutherland et al. 1994; Abu-Ashour et al. 1994; Rebata-Landa and Santamarina 2006).

Fluid permeability in sediments, which denotes the efficiency of advective transport of water and nutrients through porous media along a hydraulic gradient, is also markedly affected by a variety of interrelated environmental factors, which in turn affect the nature of microbial communities in situ. In addition to water and nutrients, small microbial cells and particulate organic matter are transported through the more permeable sandstones (Raiders et al. 1986; Huettel and Gust 1992). Impermeable layers act as barriers or cap rocks that limit the transport of fluids and solid materials, including microbial cells (Jørgensen 2000).

Porosity, pore size distribution, and grain size determine the permeability, and potentially constrain the physical extent of the deep microbial biosphere (Rebata-Landa and Santamarina 2006). Sandy sediments, which are coarser than fine clay particles, are considered to harbor denser microbial populations than clay sediments (Phelps et al. 1994; Inagaki et al. 2004). Thus, in the deep sedimentary biosphere, microbial metabolic activity has been detected in terrestrial sandstone sediments with pore sizes of $>0.2 \mu\text{m}$, while no activity was observed in shales with pore sizes of $<0.2 \mu\text{m}$ (Fredrickson et al. 1997). The critical size limit of about $0.2 \mu\text{m}$ is quite similar to the lower size limit for typical living cells, which ranges from 0.3 to $0.5 \mu\text{m}$ in diameter for spherical cells and $<0.2 \mu\text{m}$ for rod-shaped cells. Interestingly, the majority of seafloor cells are considered to have diameters of 0.25 to $0.7 \mu\text{m}$ (Kallmeyer et al. 2012). Microbial cells cannot be found in micropore spaces smaller than the cells themselves; indeed, a previous study suggested that the pores in sediments need to be approximately twice the size of a cell in order to facilitate the transport of microbial cells in subsurface environments (Updegraff 1983). Smaller cells are consequently better adapted to life in narrow pore spaces in the deep sedimentary biosphere (0.1 to $0.2 \mu\text{m}$; Schulz and Jørgensen 2001). Thus, pore size is one of the major factors affecting microbial cell abundance and microbial activity in deep shale-sandstone sedimentary environments.

Expedition 337 of the Integrated Ocean Drilling Program (IODP) was conducted by the riser drilling vessel *Chikyu* at Site C0020 near the Western Pacific margin off Shimokita Peninsula, Japan. The primary scientific objective of Expedition 337 was to investigate deeply buried microbial communities in lignite coal-bearing sediments down to a depth of 2466 m below the seafloor (mbsf), and to characterize their biogeochemical role in carbon cycling (Inagaki et al. 2012, 2015). The microbial cell abundance decreased sharply in deep sediment layers below 1200 mbsf, with most sediment

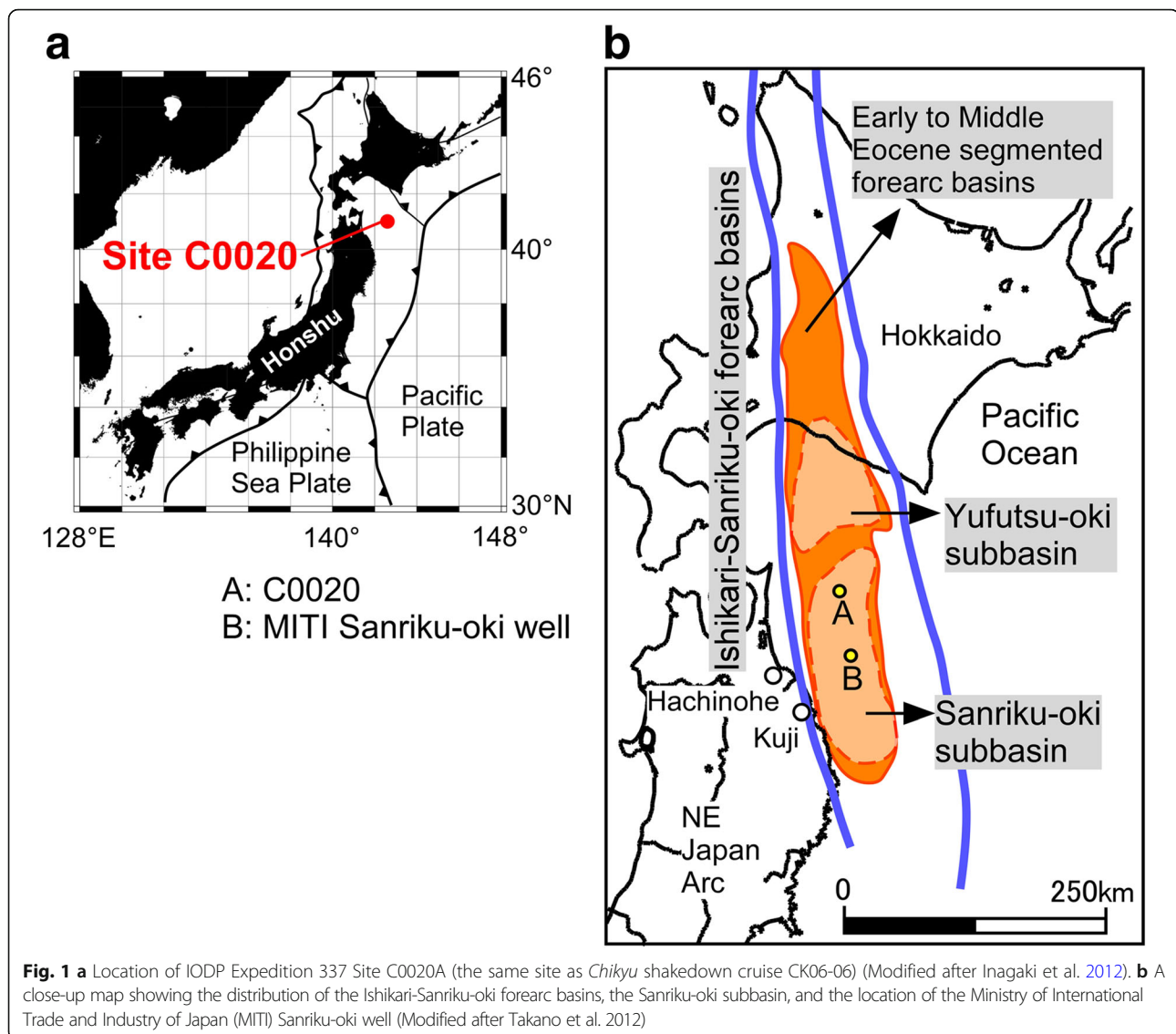
samples containing a maximum of several hundred microbial cells per cubic centimeter (Inagaki et al. 2015). However, a larger microbial biomass was observed in lignite coal layers. Physical and chemical characteristics of the cored sediment samples were determined at onboard and offshore laboratories (Gross et al. 2015; Glombitza et al. 2016; Tanikawa et al. 2016; Ijiri et al. 2017; Trembath-Reichert et al. 2017), but the key factors responsible for constraining the vertical distribution of the microbial populations in the deep sedimentary biosphere have not yet been well clarified (Hinrichs and Inagaki 2012). While permeability and pore characteristics potentially govern not only microbial biomass but also the reservoir capacity of microbially produced coalbed methane (Gamson et al. 1993; Clarkson and Bustin 1996; Strapoć et al. 2011), the transport dynamics associated with these characteristics have not yet been reported.

In this study, to determine the key physical properties that influence the habitability for microbial life of deep seafloor environments, we present the permeability and pore size distribution of core samples obtained from the coal-bearing sedimentary basin off Shimokita Peninsula, Japan (Sanriku-oki subbasin), obtained during IODP Expedition 337. The variations in the permeability and pore characteristics of sediments were investigated to clarify whether the decreasing trend in microbial cell abundance with increasing sediment depth could be explained, at least in part, by depth-dependent physical properties (Rebata-Landa and Santamarina 2006). The relationship among permeability, lithology, porosity, and pore size distribution in the sediment core samples was examined in order to clarify the factors that affect fluid transport and microbial cell abundance in the approximately 2.5-km-deep seafloor sedimentary biosphere.

Methods/Experimental

Core materials

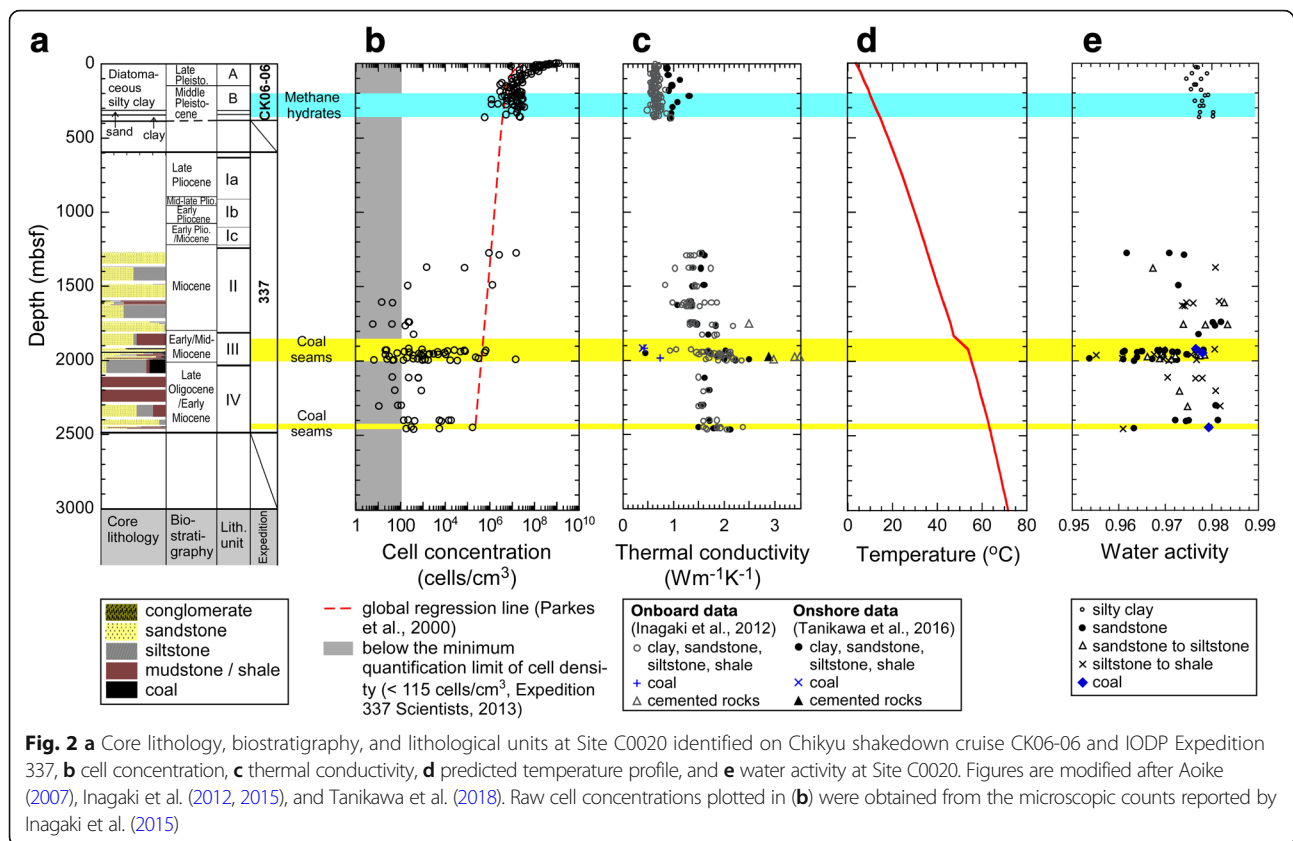
Riser drilling site C0020 off the Shimokita Peninsula, Japan, is located in a sedimentary forearc basin off the Sanriku Province that developed along the Ishikari-Sanriku-oki forearc zone, which extends along the N-S trending narrow zone from southern Hokkaido to off Kuji in Iwate Prefecture (Fig. 1, Takano et al. 2013). Gas exploration drilling by the Ministry of International Trade and Industry of Japan (MITI) confirmed the presence of an exploitable amount of natural gas in Cretaceous to Eocene coal formations in the Sanriku-oki subbasin (Fig. 1b, Osawa et al. 2002). Scientific ocean drilling was conducted near the MITI sites in the Sanriku-oki basin approximately 80 km offshore from Hachinohe City during *Chikyu* shakedown cruise CK06-06 (Expedition 902) in 2006 (Aoike 2007) and IODP Expedition 337 in 2012 (Inagaki et al. 2012). Using a non-riser hydraulic piston coring system, the initial shakedown cruise CK06-06 recovered shallow



sediment core samples from the seafloor down to 365 mbsf in Hole C9001C at Site C9001 (41° 10.5983' N, 142° 12.0328' E, water depth 1180 m), and then established a riser pilot hole (Hole C9001D) down to 647 mbsf (Aoike 2007; Masui et al. 2008). IODP Expedition 337 drilled deeper in the same riser hole (the C9001D riser hole was designated IODP Hole C0020A, and the site name was changed from Site C9001 to Site C0020). During Expedition 337, deep-sediment core samples were retrieved from 1276.5 to 2466 mbsf with riser drilling, and well logging data were acquired at the same depth interval (Fig. 2a).

Shallow sediment core samples from 0 to 340 mbsf (units A and B in Hole C9001C) obtained during cruise CK06-06 were composed mainly of unconsolidated olive-black or dark olive-gray diatomaceous silty clays, containing quartz, plagioclase, and clay minerals (Aoike

2007). Gas hydrates were observed patchily in volcanic ash and sandy sediments from ~190 to 360 mbsf (Tomaru et al. 2009). During Expedition 337, a variety of lithologies was observed in core samples collected from the deeper horizons (e.g., coal, shale, siltstone, sandstone, beach sand, carbonate cemented sandstone, and conglomerates) (Fig. 2a, Inagaki et al. 2012). Unit I, a Pliocene unit at 647 to 1256.5 mbsf, primarily comprised diatom-bearing silty clay. Unit II, a Miocene unit at 1256.5 to 1826.5 mbsf, mainly comprised silty shales intercalated with sandstone and siltstone layers. Unit III, an early to middle Miocene unit at 1826.5 to 2046 mbsf, comprised coarse- to fine-grained clastic deposits with 13 lignite coal layers (Inagaki et al. 2012; Gross et al. 2015). The coal seams in unit III were typically approximately 1 m thick, with the exception of two layers that are 3.5 and 7.3 m thick. Unit IV, an early Miocene to late



Oligocene unit at 2046.5 to 2466 mbsf, was composed of silty shale, and sandstone intercalated with siltstone and shale. A single 0.9 m thick coal seam was observed at 2449 mbsf near the base of the unit (Inagaki et al. 2012).

The total organic carbon (TOC) in coal and coaly shale (40–76 wt.%) was significantly higher than that in shale (0.43 ± 0.29 wt.%), sandstone (0.26 ± 0.18 wt.%), and shallow clay-rich silty sediments (1.2 ± 0.44 wt.%, 0 to 363 mbsf) (Aoike 2007; Inagaki et al. 2012; Gross et al. 2015). Concentrations of CO and total nitrogen dissolved in a sediment core and measured by the extraction method were higher in the coal-bearing units (1900 to 2000 mbsf, and ~2450 mbsf) than those in the adjacent sediments (Expedition 337 Scientists 2013). The depth profile for the C_1/C_2 hydrocarbon gas ratio estimated by mud-gas monitoring suggested the enhancement of microbial methane in the coal-bearing units (Inagaki et al. 2012).

Microbial cell concentrations at Site C0020 measured during CK06-06 (Morono et al. 2009) and Expedition 337 (Inagaki et al. 2015) showed that, at depths shallower than 365 mbsf, cell concentrations were considerably high (Morono et al. 2009), whereas cell concentrations in deeper layers decreased sharply below the expected global regression line (Fig. 2b; cf. Parkes et al. 2000; Inagaki et al. 2015). Nevertheless, lignite coal samples from two lithological units (unit III and the bottom of unit IV) showed

cell concentrations that were two to four orders of magnitude higher than those in the adjacent sediments (Inagaki et al. 2015).

The thermal conductivity increased gradually with depth, and this trend was explained by the reduction in porosity associated with sediment compaction during burial (Fig. 2c, Tanikawa et al. 2016). The scatter in thermal properties observed in the same horizontal section is most likely due to the high variation in the lithology at Site C0020. A temperature-depth profile at Site C0020 indicated that the temperature at the bottom of the hole was 63.7 °C (Fig. 2d; Tanikawa et al. 2016).

The water activity (A_w), a measure of how efficiently pore water facilitates biological (i.e., enzymatic) reactions, is defined as the ratio of the vapor pressure of core samples to that of pure water (Grant 2004). The water activity for the sediment core samples at Site C0020, measured using a commercial A_w sensor, ranged from 0.954 to 0.983 (Tanikawa et al. 2018) and showed no clear correlation with depth or cell concentration in the sediment sample (Fig. 2e). The A_w values in coal layers (0.977 to 0.979) were slightly lower than those in shallow sediments, but tended to be higher than those in sandstone and siltstone layers.

The sediment core samples used in this study were obtained from Hole C0020A during IODP Expedition 337 and from Hole C9001C during cruise CK06-06. We

selected core interiors for analysis to eliminate the likelihood of contamination by drilling mud from the core exteriors (Inagaki et al. 2012; Expedition 337 Scientists 2013).

Analytical methods

All of the physical properties of the core samples were measured at the Kochi Core Center.

Pore size distribution

The pore size distribution for core samples was evaluated by mercury injection capillary pressure (MICP) measurements at room temperature (25 °C) using a mercury porosimetry analyzer (PoreMaster 60 GT, Quantachrome Instruments, FL). To measure the wide range of pore sizes in sediment core samples with high accuracy, a PoreMaster 60GT with low- and high-pressure stations and dual high-pressure transducers was used. Briefly, the mercury intrusion pressure ranged from 7 to 350 kPa and from 140 kPa to 206 MPa (420 MPa for several core samples) for the low- and high-pressure stations, respectively. These pressures were used to measure pore diameters in the range of about 0.004 to 1000 μm . Before measuring the pore size distribution, sediment core samples were dried at room temperature for 72 h and then vacuum-dried for 1 week. An assemblage of two to five fragments that gave total grain matrix volumes of 0.12 to 0.68 cm^3 (i.e., 0.3 to 1.8 g) was used for each measurement.

The pore size into which mercury intrudes in core samples is given by the Washburn equation:

$$P_m \times (d/2) = -2\gamma\cos\theta, \quad (1)$$

where P_m is the injected mercury pressure, d is the pore diameter, γ is the surface tension of mercury, and θ is the contact angle between the mercury and the sample. To evaluate the pore size distribution from Eq. (1), we selected 480 erg/cm^2 (1 $\text{erg}/\text{cm}^2 = 10^{-3} \text{ N}\cdot\text{m}/\text{m}^2$) as the surface tension and a contact angle of 140° (León y León 1998). The motor speed for pressure generation was set to 5 (the motor speed of the PoreMaster 60 GT system is variable from 1 [slowest] to 25 [fastest]) in fixed rate mode, which corresponds to a generation speed of around 37 MPa/min, for high-pressure analysis. For low-pressure analysis, we were unable to control the injection pressure speed, which is around 40 kPa/min. By assuming that the intrusion volume is equivalent to the pore volume in sediments, the mercury intrusion porosity was estimated using mercury injection capillary pressure data (Filomena et al. 2012). The accuracy of the pressure transducer was $\pm 0.11\%$, and the volume change resolution was $\pm 0.0001 \text{ cm}^3$, which corresponds to a pore-size error of $\pm 0.1\%$ and a mercury intrusion porosity error of 0.01 to $\pm 0.2\%$.

Permeability measurements

The changes in permeability and porosity under high effective pressure (= confining pressure – pore pressure) were measured at room temperature (20 to 25 °C) using a high-pressure apparatus (Tanikawa et al. 2013). High confining pressure and pore fluid pressure were applied to sediment core samples to reproduce the in-situ effective pressure conditions and to estimate in-situ physical properties. All of the test samples, except for the coal samples, were cut and shaped into cylindrical forms with a length of 6 to 20 mm for permeability measurements. The cylindrical samples had faces measuring 20 mm in diameter. Since coal is very fragile, the coal samples were cut into cuboids using a small diamond cutting saw to measure the permeability. The faces of the cuboid samples measured 15 or 20 mm; i.e., the upper (inflow) and lower (outflow) faces were 15 \times 15 mm or 20 \times 20 mm.

A constant differential pore-pressure method was applied to estimate the permeability (Bernabe 1987). The following equation was used to calculate the permeability, k :

$$k = \frac{Q\eta}{A} \left(\frac{\partial P}{L} \right)^{-1} = \frac{Q\eta L}{A(P_{\text{up}} - P_{\text{down}})}, \quad (2)$$

where Q is the volume of fluid drained from the sample, A is the cross-sectional area of the sample, η is the fluid viscosity, $\delta P/L$ is the pore pressure gradient in the core samples, which is determined by the pore pressure at the upper end, P_{up} , and the lower end, P_{down} , of the specimen, and L is the length of the specimen. The inlet pore pressure was varied from 1 to 2 MPa, and the outlet pore pressure was kept constant at 1 MPa. The confining pressure and outlet pore pressure were kept constant by using an ISCO syringe pump (100DX, Teledyne ISCO Inc., Lincoln, NE), and the inlet pore pressure was controlled using a fluid/gas regulator. The same differential pore pressure (i.e., from 0.05 to 1 MPa) was applied until the flow rate, which was calculated from the change in the storage volume of the pump, became constant. The upper and lower limits for the flow rate were 10 ml/min and 5×10^{-5} ml/min, respectively, which is equivalent to a permeability of 10^{-13} to 10^{-20} m^2 for the specimen sizes in the present study. The accuracy of the pore pressure data was ± 0.001 MPa, which corresponds to $\pm 2\%$ of the maximum standard error for the permeability (the standard error for the confining pressure was ± 0.007 MPa). Pure water (Elix, Merck Millipore Corporation, Germany) was used for the pore fluid in the permeability and porosity measurements. The confining pressure was increased from 2 to 31 MPa in steps ranging in size from 1 to 10 MPa.

The pore fluid was drained from the samples to the pore fluid flow line during a stepped increase in confining pressure, and the drainage of pore fluid corresponded to the reduction in porosity. Therefore, to measure the porosity

change induced by the change in the confining pressure, the drained fluid volume was measured using the ISCO syringe pump by keeping the pore pressure constant at 1 MPa under undrained conditions (Wibberley 2002). The absolute porosity value was calculated from the change in the pore volume and the initial pore and grain matrix volumes at atmospheric pressure. The initial pore volume was calculated from the wet and dry weights of the sediment samples (the latter obtained following drying in an oven at 105 °C for 24 h), and the grain matrix volume was measured using a commercial helium gas pycnometer (Penta Pycnometer, Quantachrome Instruments, FL). The grain matrix volume was measured five times and the average value was used to calculate the initial porosity. The standard deviation of the grain matrix volume was $\pm 0.004 \text{ cm}^3$, which is equivalent to $\pm 0.3\%$ of the standard errors for the grain matrix volume and porosity.

Microstructural observations

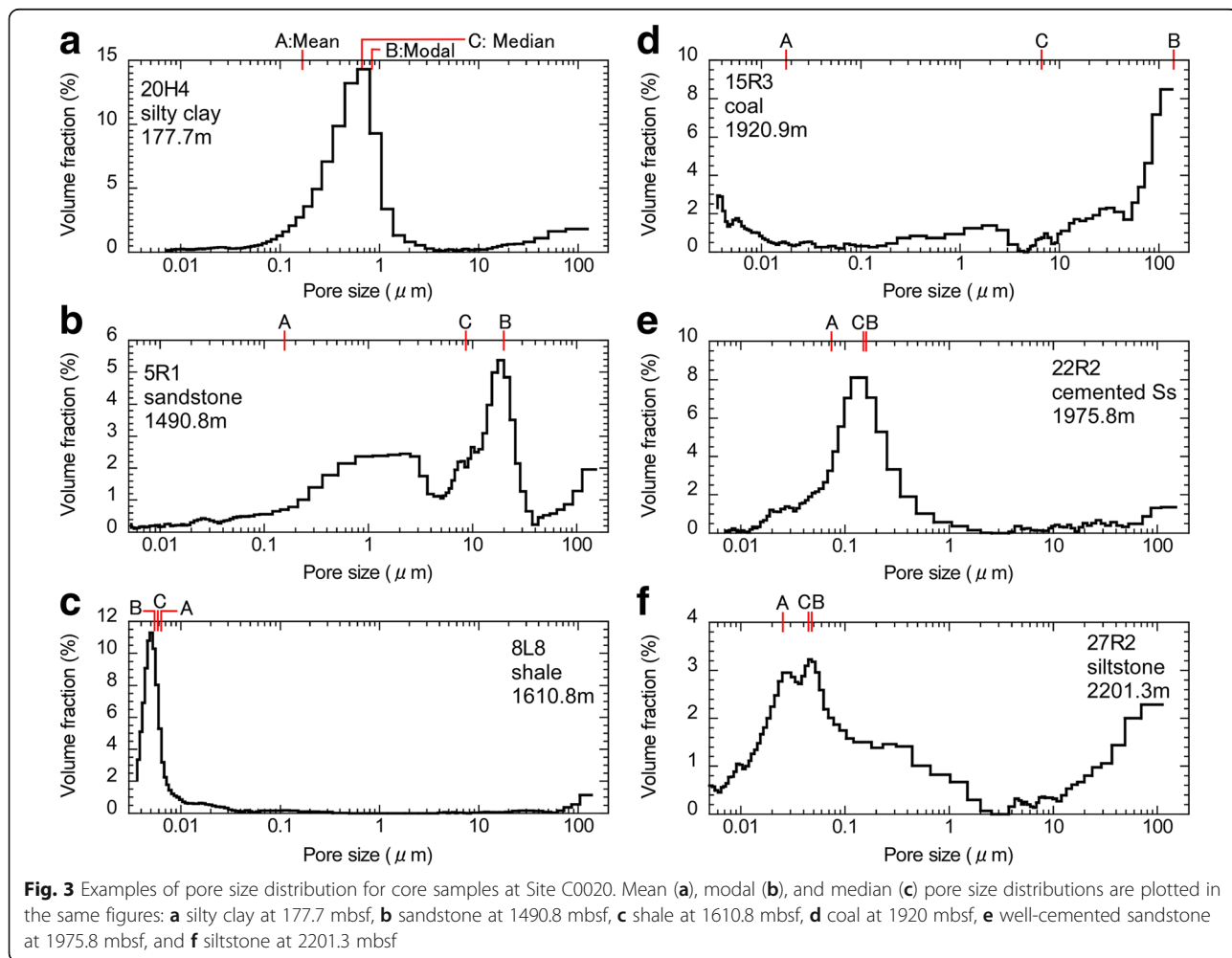
Microstructural observations of four dried samples after the permeability measurements were performed

using a micro-focus X-ray computed tomography ($\mu\text{X-CT}$) system (HMX225-ACTiSt3, Tesco Co. Ltd., Tokyo, Japan). The voltage and current used for X-ray irradiation were 90 kV and 30 μA , respectively. The resolution of the images was 1024 pixels \times 1024 pixels in a 10 mm² area (1 pixel = 10 μm). ImageJ software (<https://imagej.nih.gov/ij/>) was used to reconstruct the sliced image of the sample from the Digital Imaging and Communications in Medicine (DICOM) format data.

Results

Representative pore size distribution data

Figure 3 shows six examples of the relationship between the pore size and pore volume fraction obtained using the logarithmic pore volume distribution normalized by the total pore volume. The mean, modal, and median pore size for each treatment are given in the same figure. For unconsolidated silty clay at a shallow depth (Core 20H4, 177.7 mbsf; Fig. 3a), the unimodal pore size distribution was characterized by a single peak in the volumetric fraction at a pore size of around 0.8 μm . The results obtained



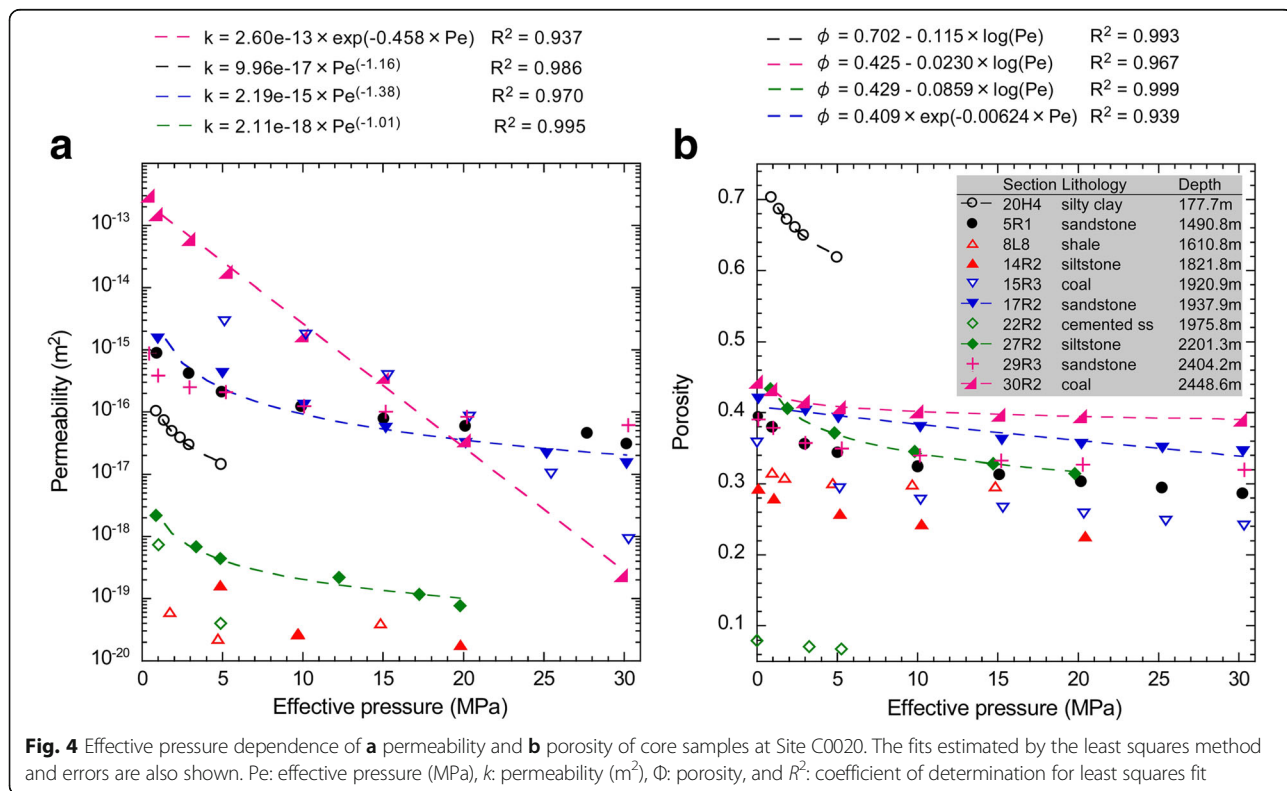
for the median pore size were similar to those obtained for the modal size, although the mean pore size was smaller than the modal size. The pore size for sandstone (Core 5R1, 1490.8 mbsf; Fig. 3b) shows a bimodal distribution characterized by two major peaks at around 2 and 20 μm, with the latter being sharper and more intense. This suggests that the larger mode corresponds to pore spaces between coarser sand grains, while the smaller mode represents those between matrix clays. The peak obtained for shale (Core 8L8, 1610.8 m; Fig. 3c) is very sharp, indicating that the pore sizes are distributed within a very narrow range centered at 0.005 μm. Both the highest and second highest volumetric fractions for the coal sample (Core 15R3, 1920.9 m; Fig. 3d) were near the highest and lowest measurable pore sizes for the experimental system. This suggests that coal has a bimodal pore size distribution with peaks at < 0.004 μm and > 100 μm. The pore size for silty clay was lower than that for sandstone, but larger than that for siltstone and shale.

Pressure dependence of transport properties

The permeability of sedimentary rock samples at an initially applied effective pressure of 1 to 3 MPa (defined as the initial permeability) varied from 10⁻¹³ to 10⁻¹⁹ m², and decreased with effective pressure in all specimens (Fig. 4a). The initial permeability of coal was the highest among the tested specimens (> 10⁻¹³ m²). At an effective

pressure of 20 MPa, the coal permeability decreased by two to three orders of magnitude from the initial permeability, while the permeability of sandstone and siltstone at an effective pressure of 20 MPa decreased by one order of magnitude. At a high effective pressure (> 20 MPa), the permeability of coal (Cores 15R3 and 30R2) was lower than that of sandstone. Among the other lithologies examined, shale showed the lowest permeability at any effective pressure, reaching the lower measurable limit (about 10⁻²⁰ m²) at an effective pressure of 10 to 20 MPa. The reduction rate for permeability with increasing effective pressure varied with lithology, and coal exhibited the highest pressure sensitivity. The reduction curve for coal permeability (Core 30R2) as a function of effective pressure could be expressed by an exponential decay function, while the permeability-effective pressure correlation for sandstone, siltstone, and silty clay could be fitted using a power-law curve with an exponent of around -1 (Fig. 4a).

The porosity decreased from the initial value at atmospheric pressure (defined as the initial porosity in this paper) by 5 to 12% at an effective pressure of 20 MPa (Fig. 4b). In all samples, the porosity reduction rate decreased with increasing effective pressure, and the reduction curves could be fitted using logarithmic and exponential curves. Among the specimens tested, the reduction rate for porosity was the highest for the silty clay samples (Core 20H4, 8.5% reduction at an effective pressure of 5 MPa), and the lowest for carbonate



cemented sandstone (Core 22R2, 1.2% reduction at 5 MPa) and shale (Core 8L8, 1.5% reduction at 5 MPa).

Depth profile of physical properties

The experimental results showed that the permeability for all specimens decreased with increasing effective pressure (Fig. 4a). Therefore, the laboratory results for the permeability-effective pressure profiles were used to estimate the depth profiles for the in-situ permeability (defined as the permeability at an effective pressure that is equivalent to the depth of the core samples in this study) at Site C0020. According to Wangen (1997), the vertical effective pressure (Pe) at a depth z = h below the seafloor under hydrostatic pressure is defined as

$$Pe = \int_0^h \rho_b g \delta z - \int_0^h \rho_f g \delta z \tag{3}$$

$$= \int_0^h [(1 - \Phi(z))\rho_r + \Phi(z)\rho_f] g \delta z - \int_0^h \rho_f g \delta z,$$

where $\Phi(z)$ is the porosity at depth z, ρ_b is the wet bulk density, ρ_r is the grain density, ρ_f is the fluid density, and g is the gravitational acceleration. The porosity-depth relationship at this site was reported in a previous study (Tanikawa et al. 2016), and is characterized by a negative exponential curve:

$$\Phi = \Phi_0 \exp(-\alpha z), \tag{4}$$

where Φ_0 is the porosity at the seafloor (z = 0 mbsf) and α is a consolidation factor that is evaluated empirically. Values of $\Phi_0 = 0.740$ and $\alpha = 0.000456 \text{ m}^{-1}$ fit the porosity-depth curve at this site well (Fig. 5a). To

simplify the model, pore fluid pressure was assumed as hydrostatic pressure, and the grain density and fluid density were assumed to be constant at 2650 kg/m³ and 1000 kg/m³, respectively. Using the assumptions above, a 2 km depth off Shimokita corresponds to an effective pressure of 16.7 MPa. The in-situ porosity (defined as the porosity at an effective pressure that is equivalent to the depth of the core samples under hydrostatic pressure in this study) was also estimated from the pressure-porosity relationship determined in the laboratory, which is the same methodology as that employed for the permeability estimation.

The in-situ porosity results obtained in this study generally agreed well with measurements performed at atmospheric pressure onboard, as well as the logging data calculated using the gamma-ray bulk density data from the three-detector lithology density (TLD) logging tool (Fig. 5a; Inagaki et al. 2012). At larger depths, the in-situ porosity is much closer to the logging data than the onboard porosity data.

The in-situ permeability of silty clay at shallow horizons was approximately 10⁻¹⁶ m² (Fig. 5b), implying that the in-situ permeability decreases with increasing depth, although the data are highly scattered around coal-bearing layers (unit III and lower portion of unit IV). In unit III, the in-situ permeability of sandstone and coal was 4 to 5 orders of magnitude larger than that of siltstone and shale. The lowest in-situ permeability of <10⁻²¹ m² was observed in shale at around 2100 mbsf. Coal materials at around 1900 mbsf exhibited the highest in-situ permeability of 9 × 10⁻¹⁵ m², but relatively low in-situ permeability values were also obtained for other coal samples (10⁻¹⁹ m²) in the same unit III (Fig. 5b; Ijiri et al. 2017).

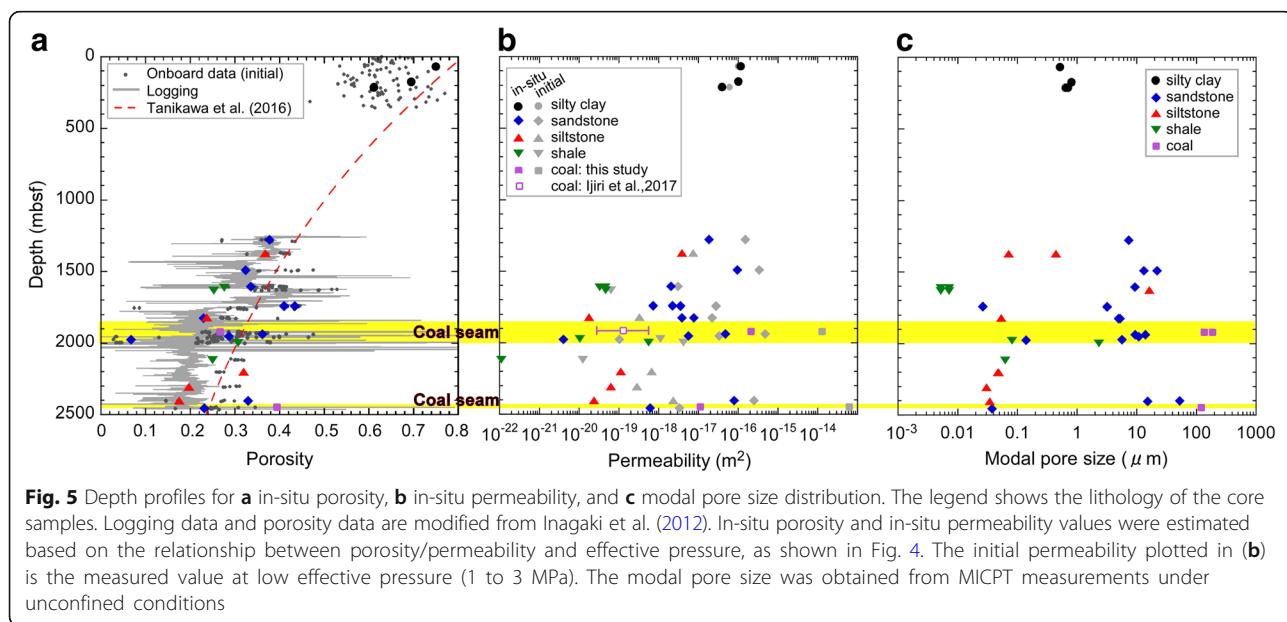


Fig. 5 Depth profiles for **a** in-situ porosity, **b** in-situ permeability, and **c** modal pore size distribution. The legend shows the lithology of the core samples. Logging data and porosity data are modified from Inagaki et al. (2012). In-situ porosity and in-situ permeability values were estimated based on the relationship between porosity/permeability and effective pressure, as shown in Fig. 4. The initial permeability plotted in (b) is the measured value at low effective pressure (1 to 3 MPa). The modal pore size was obtained from MICPT measurements under unconfined conditions

Since the pore size distribution was measured under unconfined conditions, the depth profile of pore size that we determined in the present study tended to yield values that were larger than in-situ values. The depth profile for the pore size shows that the pore size is highly scattered due to lithological variation; for example, the pore size for sandstone, siltstone, and coal layers ranges from 3 to 30 μm , 0.03 to 0.1 μm , and 100 to 200 μm , respectively (Fig. 5c). No pore size dependence on depth was observed for any of these lithologies. The smallest pore size of around 0.01 μm was observed for shale at 1600 mbsf, while the largest pore size was observed for coal samples at 1900 mbsf, which is in good agreement with the horizons at which high in-situ permeabilities were observed.

Relationship between cell abundance and physical properties

The correlation between cell abundance and in-situ physical properties is plotted in Fig. 6, using the cell concentration data obtained from microscopic direct counts (Morono et al. 2009; Inagaki et al. 2015). The depth profile for cell concentration at Site C0020 was compiled using data from core samples collected at depths closest to those used for our laboratory experiments.

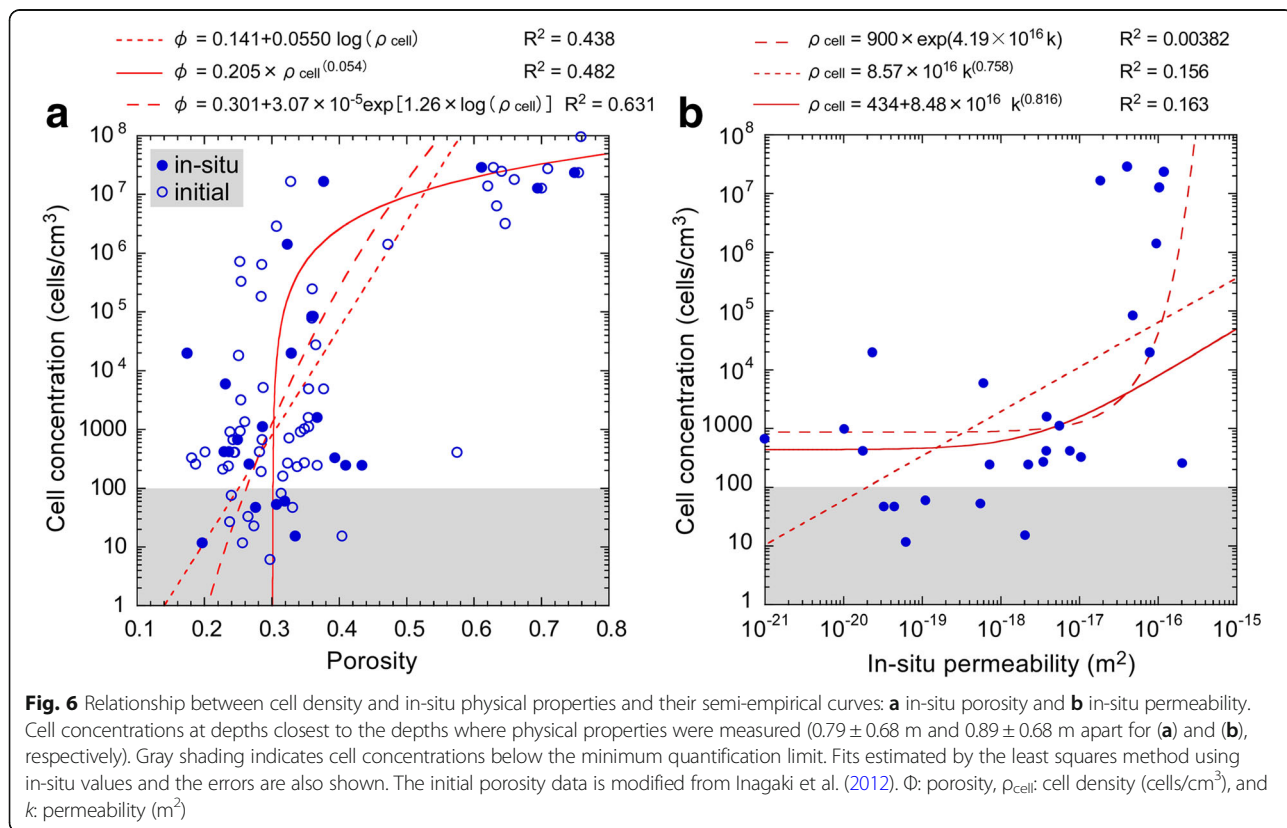
Despite not having sufficient data for in-situ porosities in the range of 0.45 to 0.6, the cell concentration appeared to decrease with decreasing in-situ porosity (Fig. 6a). The

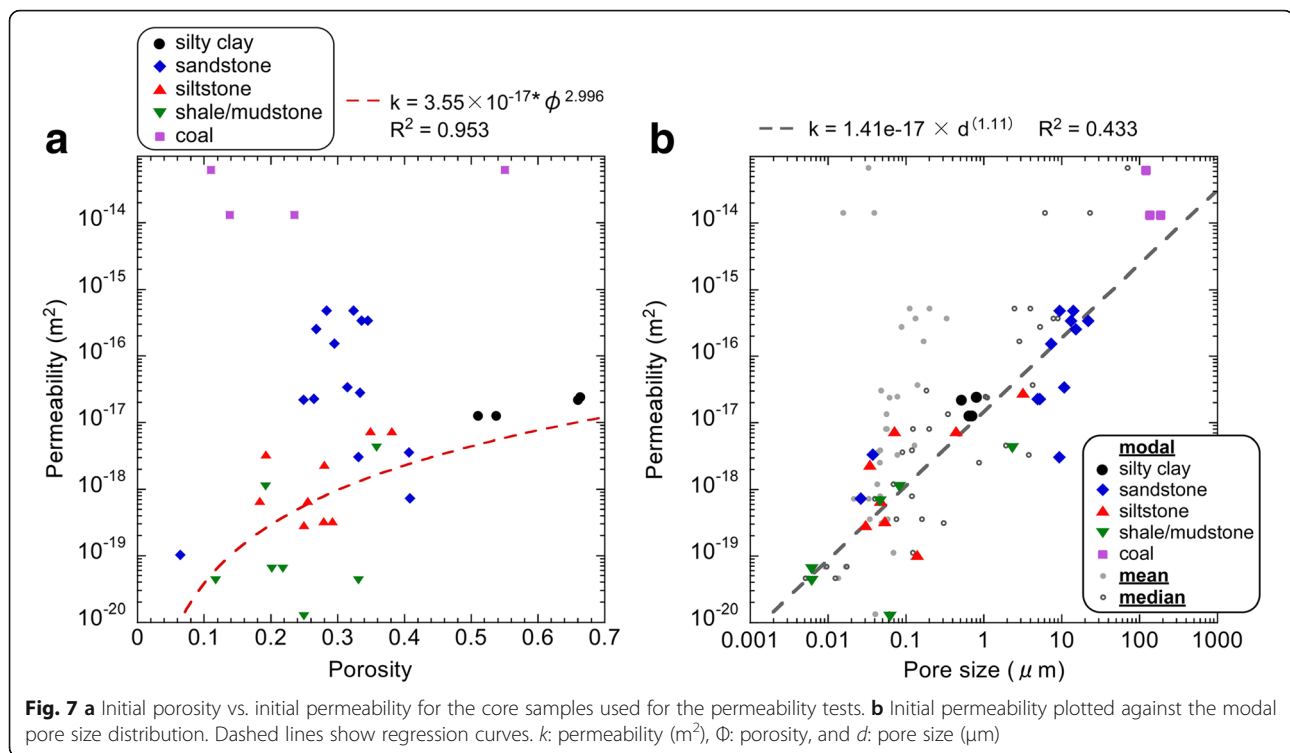
correlation between the decrease in in-situ porosity and the logarithmic decrease in cell concentration with depth could be well described by an exponential decay function, which is similar to the function employed for the porosity-depth reduction curve described by Eq. (4). However, in the low in-situ porosity range ($< \sim 0.4$), no clear influence of in-situ porosity on cell concentration in our dataset was observed.

In-situ permeabilities above 10^{-17} m^2 were correlated with higher cell concentrations ($> 10^4 \text{ cell/cm}^3$), and cell abundance decreased markedly for in-situ permeabilities of less than 10^{-17} m^2 (Fig. 6b). This relationship was well described by a power-law function and/or an exponential decay function. However, no clear dependence of the in-situ permeability on the cell concentration was observed for the low-permeability samples. In these samples, the correlation between cell density and pore size was more complicated, and no well-defined relationship was observed (Additional file 1: Figure S1).

Relationship among initial porosity, initial permeability, and pore size

No obvious correlation was observed between the initial porosity and the initial permeability (Fig. 7a). However, the effect of the lithology on the cross-plot data is apparent; e.g., coal has a very high initial permeability, which is independent of the initial porosity, and the dependence of





the initial permeability on the initial porosity is very weak for sandstone. Silty clay has a high initial porosity and a relatively low initial permeability, and the initial permeabilities of siltstone and shale show a slight initial porosity dependence. The fitting curves based on the integrated initial porosity data for silty clay, siltstone, and shale—all of which are classified as fine-grained materials—are described by a power-law function with an exponent of ~ 3 .

The initial permeability was found to decrease with decreasing modal pore size (Fig. 7b). This relationship was well fit by a power-law function for all lithologies. The coal group has a large pore size and a high initial permeability, while shale has a small pore size and a moderately low initial permeability. The relationship between the median pore size and the initial permeability is similar to that for the modal pore size, whereas the mean pore size is less dependent on the initial permeability (Fig. 7b).

Microstructure

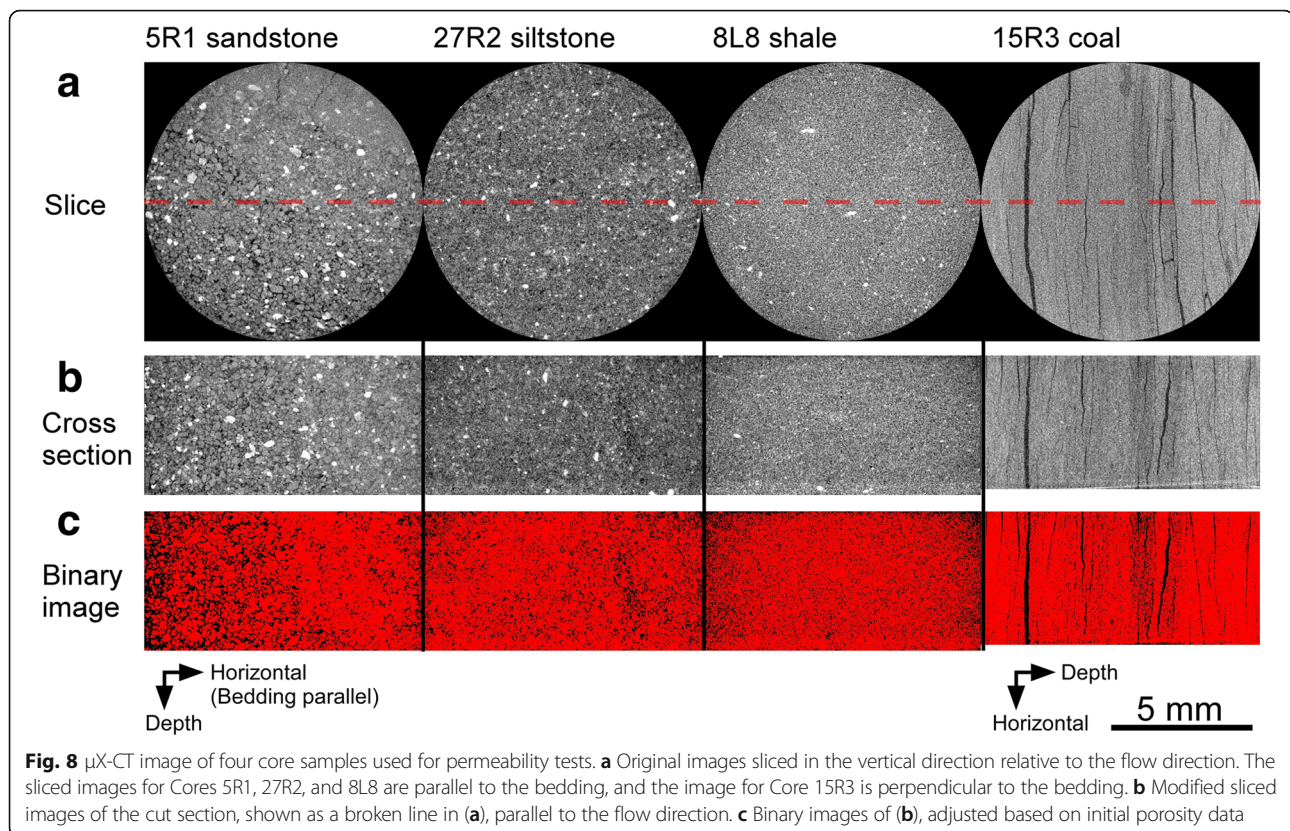
Microstructural observations by $\mu\text{X-CT}$ showed that sandstone (Core 5R1; Fig. 8) consists of a mixture of coarse particles (0.1 to 0.2 mm in diameter) and very fine particles that fill some of the pores between the larger grains. This leads to the bimodal pore-size distribution seen in Fig. 3b, with a broad peak at about 2 μm and a sharper and more intense peak at about 20 μm . This suggests that the larger mode corresponds to pore spaces between coarser sand grains, while the smaller mode represents those between matrix clays.

The pore size for the sandstone in Fig. 8b is the largest among the four samples. The siltstone (Core 27R2) and shale (Core 8L8) exhibit smaller pore sizes, and the pores are more homogeneously distributed. The $\mu\text{X-CT}$ analysis revealed that the coal sample (Core 15R3; Fig. 8) has open parallel cracks, or cleats (see Laubach et al. 1998 for naturally occurring fractures). Most cleats developed in the direction parallel to the horizontal bedding plane, but a small number also formed in the vertical direction, and in so doing, connected fractures oriented parallel to the bedding itself (Fig. 8a). The aperture size of the cleats ranged from < 10 to 100 μm . Isolated pores in the coal matrix were very small, and the $\mu\text{X-CT}$ images showed that the average density of vertical fractures was around 1 fracture/mm.

Discussion

Which physical factors affect depth-dependence of microbial cell abundance?

Both the porosity and the permeability decrease with increasing effective pressure (Fig. 4), and the correlation between the initial porosity and the initial permeability for fine-grained sediments is well defined (Fig. 7a). The increasing compaction of sediments with depth results in reduced porosity and permeability, which may correspond to lower tortuosity and lower pore connectivity. Increasing compaction may thus constrain the habitability of deep sediments for microbial communities (Prasad 2003; Rebata-Landa and Santamarina 2006). Compaction is also



likely to influence the transport of water, nutrients, and secondary products of microbiological activity (Yakimov et al. 1997). Therefore, the positive correlation between cell concentration and in-situ porosity observed at Site C0020 suggests that mechanical sediment compaction was responsible for the low density of microbes at this site (Figs. 2a and 6a). Indeed, the positive correlation between cell concentration and in-situ permeability also supports this notion (Fig. 6b). The influence of sediment compaction on cell abundance would be more apparent in shallower environments than in deeper environments, as the variation in cell concentration is less constrained in the low in-situ porosity and in-situ permeability regimes.

Why do coal-bearing units have anomalously high microbial biomass?

At Site C0020, the coal-bearing sections in unit III and the lower portion of unit IV had relatively high microbial cell concentrations. These units/sections were characterized by having relatively permeable coal and sandstone layers with a relatively large pore size (Fig. 5b, c). The changes that occur with increasing depth, which are mainly due to variations in the lithology, are larger for the permeability and the pore size than for the porosity. Consequently, because of the large variation in lithology at Site C0020, there was no clear correlation between the porosity and the permeability below 1000 mbsf (Fig. 7a).

The large pore size determined by MICP for coal likely reflects the existence of voids in the fractures (cleats). Consequently, the high permeability of coal at low effective pressure likely has a marked influence on both vertical and bedding parallel flow through cleats. The permeability of coal is very sensitive to the effective pressure, and the in-situ coal permeability can be very different to the initial permeability. Therefore, the in-situ pore size (aperture size) for coal is expected to be much smaller than the measured pore size (Fig. 7b). Nevertheless, voids in fractures may form an important pathway for fluid flow through coalbeds, because the in-situ permeability of fractured coal is much higher than that of the intact coal matrix or neighboring siltstone/shale formations (Fig. 5b, Ijiri et al. 2017). Therefore, it is considered that nutrients and energy sources were mainly released from the coal layers through the cleats, where large amounts of energy sources are stored, and that these compounds seeped into the overlying permeable sandy sediments. However, the impermeable shale and siltstone layers, which overlie the permeable sandstone layers, may act as barriers to vertical fluid flow. As shown in Fig. 5b, the permeability change between permeable (sandstone, coal) and impermeable (siltstone, shale) layers was two to four orders of magnitude in coal-bearing units. Since almost no nutrient flow occurs through the impermeable layer, the very low cell densities at 1500 to 1800 mbsf and from 2000 to 2400

mbsf (< 100 cells/cm³) can be explained by the effectiveness of the siltstone barrier for preventing the vertical transport and dispersal of nutrients and cells. Permeable layers may sustain more abundant active microbial populations than low-permeability layers, and may be one of the reasons for the higher cell numbers in coalbed layers (Inagaki et al. 2015). Therefore, in deeper sections, pore size and permeability, rather than porosity, are considered to have a greater influence on cell abundance (Phadnis and Santamarina 2011).

The in-situ permeability was estimated from the effective pressure dependence of the permeability, assuming that the pore pressure is hydrostatic in deep regions. However, overpressure (pore pressures higher than the hydrostatic pressure) occurs in deeper regions of most thick sedimentary/petroleum basins (Bredehoeft and Hanshaw 1968; Swarbrick and Osborne 1998) and in coal sediments (Law 1984; Su et al. 2003). Since siltstone and shale at Site C0020 form an impermeable barrier to fluid migration, overpressure in and below impermeable formations can easily occur due to inhibition of vertical fluid/gas transfer and hydrocarbon generation in coal units (Hunt et al. 1994, 1998; Osborne and Swarbrick 1997; Zhao et al. 2018). The permeability of coal is much more sensitive to the effective pressure than that of other rock types in the Sanriku-oki subbasin. Therefore, overpressure would be expected to increase the in-situ permeability and pore size for coal, so allowing an abundant microbial population to be sustained. Overpressure can also increase the methane sorption and storage capacity of coal (Scott 2002).

In the past, the shale layer may have supplied organic matter that was consumed by microbes in the adjacent sandstone layers (Fredrickson et al. 1997). However, because the shale deposits at Site C0020 currently have a much lower TOC content and a lower diffusion rate than those for coal, the nutrients that support indigenous microbial communities in sandstone and coal are considered to be derived from lignite coal. Cleats and fractures in coal increase the substrate surface area available for microbial action (Strapoć et al. 2011). Since young lignite coal is susceptible to microbial attack, microbial coalbed methane would have been readily produced in the coalbeds of the Sanriku-oki basin.

Influence of pore size on sedimentary microbial biomass

Pore size can restrict both the size of microbial populations and the cellular volume in porous sediments (Fredrickson et al. 1997). At Site C0020, the modal pore size for shale (0.028 ± 0.035 μm) and siltstone (0.044 ± 0.009 μm) adjacent to coal units is less than 0.2 μm (Fig. 5c), whereas the pore size for sandstone and coal is > 2 μm (fracture aperture size of > 1 μm). A pore size of 0.2 μm for lithologies with low in-situ permeability

is consistent with the proposed threshold size for microbial metabolic activity (Fredrickson et al. 1997). The pore size for shale and siltstone is probably smaller than the majority of in situ microbial cells at C0020, since microbial cells in deep marine sediments are approximately 0.5 μm in size (Kallmeyer et al. 2012; Braun et al. 2016), and the microbial cell size estimated after incubating coal and shale samples from C0020 ranged from 0.3 to 1.2 μm (Trembath-Reichert et al. 2017). If the pore size is smaller than the cell size, then cell dispersal will not occur despite the presence of intense hydrological fluid flows, and microbial activity in such sediments will be low.

At Site C0020, it is conceivable that microbial cells were buried and trapped in shale and siltstone, promoting the agglutination of cells, and limiting the physical transport and/or migration of cells and eukaryotic spores from sandstone and coal layers to shale and siltstone layers (Inagaki et al. 2015; Gross et al. 2015; Liu et al. 2017).

Other potential geophysical constraints on deep subseafloor microbial biomass

In addition to the physical properties of sedimentary rock, other environmental factors also affect the microbial habitability of the deep subseafloor biosphere, e.g., temperature, pressure, water content, A_w , pore fluid chemistry, and pH (Beuchat 1974; Fernández Pinto et al. 1991; Zhang et al. 1998; Jenkins et al. 2002; Musslewhite et al. 2003; Grant 2004; Williams and Hallsworth 2009; Stevenson et al. 2015). These different geophysical parameters control the availability of nutrients and energy substrates required for the maintenance of essential cellular functions (e.g., biomolecule repair) over geological time (Hoehler and Jørgensen 2013; Lever et al. 2015).

In general, soil bacteria exhibit optimal growth at high A_w , but several bacteria have a high tolerance to desiccation ($A_w < 0.8$, Griffin 1972; Lavelle and Spain 2001) and highly saline water ($A_w \approx 0.61$, Grant 2004). The A_w values at Site C0020A range from 0.954 to 0.983 and are almost unaffected by depth or lithology (Fig. 2e, Tanikawa et al. 2018). Since the A_w values are considerably higher than the A_w limit for the biosphere, water activity is not considered to affect the microbial population size or activity in the Sanriku-oki subbasin.

Although the temperature at Site C0020 increases almost linearly with depth (24.4 $^{\circ}\text{C}/\text{km}$, Tanikawa et al. 2016), it is not clear whether such temperature increases limit the population size, activity, or microbial community structure in the deep subseafloor biosphere (Hinrichs and Inagaki 2012).

Permeability estimates based on pore characteristics

Our results indicate that differences in pore size are mainly responsible for the observed variation in initial permeability (Fig. 7b). To date, numerous attempts have

been made to relate the pore size distribution and the porosity to the fluid permeability (Dullien 1992). The relationship between the initial porosity and initial permeability also indicates that the permeability characteristics of fine-grained sediments are governed by the traditional Kozeny-Carman equation (Fig. 7a). This equation is widely applied to mathematical models of microbiological processes (Taylor et al. 1990; Vandevivere et al. 1995) or prediction of permeability in well logging tools (Prasad 2003; Osterman et al. 2016). The formula describes the relationship between the permeability and the pore size, porosity, and geometry of porous sediments based on the assumption that the pore structure consists of a bundle of cylindrical capillaries (Dullien 1992). The Kozeny-Carman equation is expressed as follows:

$$k = \frac{\Phi d^2}{16f\tau^2}, \quad (5)$$

where k is the permeability, ϕ is the porosity, d is the diameter of a volume-equivalent spherical pore, f is a factor that accounts for pores with different cross-sectional shapes, τ is the tortuosity factor, and $f\tau^2$ is the Kozeny-Carman coefficient. In this study, the mercury intrusion porosity and representative pore size evaluated from the MICP measurements were used to calculate the permeability based on Eq. (5), where f was assumed to have a value of 2.

Poremaster software (Poremaster for Windows® 8.01, Quantachrome Instruments, FL) was used to calculate the tortuosity values from the MICP measurement results. The empirical formula introduced by Carniglia (1986) is based on Fick's first law and a cylindrical pore structure model, and is expressed as follows:

$$\tau = (2.23 - 1.13V\rho_b) \left[0.92 \times \frac{4}{S} \sum \left(\frac{v_i}{d_i} \right) \right]^{1+\varepsilon}, \quad (6)$$

where V is the total specific pore volume, ρ_b is the bulk density of the sediment, S is the total surface area of sediment particles, v_i is the change in pore volume within a pore size interval i , d_i is the average pore size within a pore size interval i , and ε is the pore shape factor exponent ($0 < \varepsilon < 1$). A value of $\varepsilon = 1$, which corresponds to cylindrical pores, was used in this study. To estimate the permeability using Eqs. (5) and (6), the mean, modal, and median pore sizes were used (see Additional file 1: Figure S2 and Table S1).

In the low-permeability region ($< 10^{-17} \text{ m}^2$), the permeabilities estimated using the mean and modal pore sizes were in reasonable agreement with the measured permeabilities under a low effective pressure of 3 MPa (Fig. 9). In the higher permeability region, use of the mean pore size underestimated the permeability, while use of the modal or median pore size overestimated it

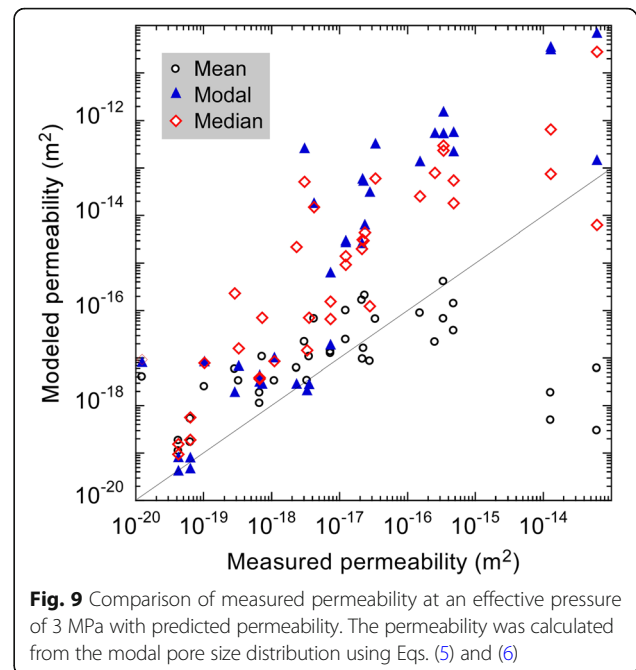


Fig. 9 Comparison of measured permeability at an effective pressure of 3 MPa with predicted permeability. The permeability was calculated from the modal pore size distribution using Eqs. (5) and (6)

(Fig. 9). The modal pore size was therefore considered to be representative of the fluid transport properties over a wide permeability range.

Fracture permeability model

Using the average pore size, the Kozeny-Carman equation (Eq. 5) did not accurately reproduce the measured permeability when the permeability was high (Fig. 9). Microstructural images of the coal material (Fig. 8, Core 15R3) showed that fluids could selectively flow through fractures; consequently, a fracture permeability model seems more appropriate than the capillary-tube-based Kozeny-Carman model. The well-known empirical equation for single fracture flow, known as the cubic law (Witherspoon et al. 1980; Raven and Gale 1985), is expressed as follows:

$$Q_{fr} = \frac{b^3 \Delta P}{12R \mu L} \quad (1.06 < R < 1.65), \quad (7)$$

where Q_{fr} is the flow rate per unit width normal to the flow direction, b is the mean aperture size of the fracture, R is a fracture surface characteristic factor, μ is the fluid viscosity, and $\Delta P/L$ is the pressure gradient in the direction of the fluid flow. Here, we consider the cuboid coal samples that were used in the permeability measurements in this study. Fracture planes develop parallel to the sample length, L , and sample width, W , and normal to the H axis. If multiple parallel fractures developed parallel to the L and W directions, then the flow rate per unit area, q , measured in the permeability tests can be expressed as follows:

$$q = \frac{Q_{fr} \times W(\rho_{fr}H)}{W \times H} = \frac{b^3 \Delta P}{12R \mu L} \rho_{fr}, \quad (8)$$

where ρ_{fr} is the fracture density (number of fractures per unit length normal to the fracture surface). Based on Eq. (2), the fracture permeability is then given by:

$$k_f = \frac{b^3 \rho_{fr}}{12R}. \quad (9)$$

The μ X-CT data for the coal sample (Fig. 8c) showed that b ranged from 1 to 10 μm , and ρ_{fr} was 1000 m^{-1} . Therefore, assuming that $R = 1$, the coal permeability approaches 10^{-13} to 10^{-14} m^2 , which is more consistent with the experimentally determined permeability than that estimated using the Kozeny-Carman model. This result suggests that fluid transport within coal is mainly affected by the fracture (or cleat) geometry, rather than by the coal matrix, for which the permeability model consists of an assembly of circular pipes.

Conclusions

To determine the key physical properties that dominate the habitability for microbial life of deep seafloor coal-bearing environments, the porosity, permeability, and pore size distribution for sedimentary rocks off the Shimokita Peninsula, Japan, were measured using core samples obtained during the *Chikyu* shakedown cruise CK06-06 and IODP Expedition 337. The porosity and permeability were measured at an effective pressure of up to 30 MPa to correct for the influence of the effective pressure. The in-situ porosity and permeability gradually decreased with increasing depth down to about 2.5 km below the ocean floor (water depth of 1180 m). However, the in-situ porosity and permeability, and the pore size for sediments at depths greater than 1200 mbsf depended strongly of the lithology. For example, the in-situ permeability and pore size for coal and sandstone are 10^{-16} to 10^{-18} m^2 and 100 to 10 μm , respectively, while those for siltstone and shale are 10^{-19} to 10^{-22} m^2 and < 0.1 μm , respectively. The higher permeability of coal at low effective pressure is due to the dominance of fracture (cleat) flow, whereas that of sandstone is due to the higher volume fraction of large pores. At low effective pressures, the measured permeability for coal conforms to the fracture permeability model, whereas that for the other lithologies is better predicted using the Kozeny-Carman equation and pore size data.

The decrease in microbial cell concentration with increasing depth in shallow sediments at Site C0020 is consistent with a reduction in in-situ porosity and permeability. This suggests that the gradual decrease in microbial biomass at shallow depths can be explained by a gradual decrease in pore connectivity and flow pathways

due to mechanical compaction. On the other hand, the cellular biomass is less dependent on the in-situ porosity and permeability at depths below 1200 mbsf. Anomalously high microbial cell concentrations ($\sim 10^{4-5}$ cells/ cm^3) were observed in coal-bearing layers comprising highly permeable sandstone and coal formations with relatively large pore sizes, whereas very low cell concentrations were observed in very low-permeability siltstone and shale formations with small pore sizes. Therefore, lithological variation of hydrological properties may control the vertical distribution of microbial biomass at greater depths. The nutrients and energy sources in lignite coals can move through the fracture (cleat) systems in the coalbeds and can reach adjacent permeable layers, resulting in locally dense microbial populations. Conversely, impermeable siltstone and shale layers that act as cap rocks for fluid transport may limit the habitability for microbial communities by suppressing the supply of water and energy-rich substrates from the permeable layers. The pore size for siltstone and shale at Site C0020 is generally < 0.2 μm , potentially limiting microbial life. Fractures in the lignite coal are likely to have promoted the production of biological coalbed methane, and in the presence of impermeable formations, this would have generated overpressure in the coalbeds, which would keep fractures open and produce large pore spaces. Based on these observations, we suggest that fluid permeability and pore size are important environmental factors that limit life in deep seafloor environments and the physical extent of the biosphere in sedimentary basins.

Additional file

Additional file 1: Figure S1. Relationship between cell concentration and modal pore size. No meaningful correlation is obtained. **Figure S2.** Depth-tortuosity profile at Site C0020. Tortuosity was calculated from Eq. (6) using mercury injection capillary pressure (MICP) data. The evaluated tortuosity was used for permeability calculations. The tortuosity estimated from Eq. (6) ranged from 1.48 to 2.16, and decreased with increasing depth, probably due to the tortuosity having a strong dependence on porosity. **Table S1.** General information and physical properties for core samples collected at Site C0020A. **Table S2.** Permeability calculated from Eqs. (5) and (6) using pore size distribution data. Data are plotted in Fig. 9. **Table S3.** In-situ porosity and permeability plotted in Fig. 5a and b. (DOC 2321 kb)

Abbreviations

A_w : Water activity; DICOM: Digital Imaging and Communications in Medicine; IODP: Integrated Ocean Drilling Program; mbsf: Meters below seafloor; MICP: Mercury injection capillary pressure; TLD: Three-detector lithology density logging tool; TOC: Total organic carbon; μ X-CT: Micro-focus X-ray computed tomography

Acknowledgements

The present research used core samples and data provided by the Integrated Ocean Drilling Program (IODP) Expedition 337. We thank the crews, scientists, and laboratory technicians aboard the *D/V Chikyu* for drilling, coring, and

sample processing during IODP Expedition 337. The manuscript had benefited from reviews by Ryuji Tada, Yasufumi Iryu, and anonymous reviewers.

Funding

This study was supported in part by the Japan Society for the Promotion of Science (JSPS) Strategic Fund for Strengthening Leading-Edge Research and Development (to JAMSTEC), the JSPS Funding Program for Next Generation World-Leading Researchers (NEXT Program, to FI), and the JSPS Grant-in-Aid for Scientific Research (No. 25800284).

Availability of data and materials

The data supporting this paper are available in the supplementary information files (Additional file 1: Figure S1 and S2, and Tables S1–S3), and at SIO7 Data Center (<http://sio7.jamstec.go.jp/>).

Authors' contributions

WT, KUH, and FI designed the study. WT and OT conducted physical property measurements and data analysis. YM performed cell counts. FI led cruise CK06-06. FI and KUH led IODP Expedition 337 and contributed to data interpretation by WT. WT and FI wrote the paper. All of the authors approved the final version of the manuscript.

Competing interests

The authors declare that they have no competing interests.

Publisher's Note

Springer Nature remains neutral with regard to jurisdictional claims in published maps and institutional affiliations.

Author details

¹Kochi Institute for Core Sample Research, Japan Agency for Marine-Earth Science and Technology (JAMSTEC), Monobe B200, Nankoku, Kochi 783-8502, Japan. ²Research and Development (R&D) Center for Submarine Resources, JAMSTEC, 2-15 Natsushima-cho, Yokosuka, Kanagawa 273-0061, Japan. ³Marine Works Japan Ltd., Monobe B200, Nankoku, Kochi 783-8502, Japan. ⁴MARUM Center for Marine Environmental Sciences and Department of Geosciences, University of Bremen, 28359 Bremen, Germany. ⁵R&D Center for Ocean Drilling Science (ODS), JAMSTEC, Yokohama, Kanagawa 236-0001, Japan.

Received: 23 August 2017 Accepted: 12 September 2018

Published online: 26 September 2018

References

- Abu-Ashour J, Joy DM, Lee H, Whiteley HR, Zelin S (1994) Transport of microorganisms through soil. *Water Air Soil Pollut* 75:141–158. <https://doi.org/10.1007/BF01100406>.
- Aoike K (ed.) (2007) CK06-06 D/V Chikyū shakedown cruise offshore Shimokita: Laboratory Operation Report. CHIKYU Cruise report. http://www.godac.jamstec.go.jp/catalog/data/doc_catalog/media/CK06-06_902_all.pdf.
- Bernabe Y (1987) A wide range permeameter for use in rock physics. *Int J Rock Mech Min Sci Geomech Abstr* 24:309–315. [https://doi.org/10.1016/0148-9062\(87\)90867-9](https://doi.org/10.1016/0148-9062(87)90867-9).
- Beuchat LR (1974) Combined effects of water activity, solute, and temperature on the growth of *Vibrio parahaemolyticus*. *Appl Microbiol* 27:1075–1080.
- Braun S, Morono Y, Littmann S, Kuypers M, Aslan H, Dong M, Jørgensen BB, Lomstein BA (2016) Size and carbon content of sub-seafloor microbial cells at Landsort deep, Baltic Sea. *Front Microbiol* 7:1375.
- Bredehoeft JD, Hanshaw BB (1968) On the maintenance of anomalous fluid pressures: I. thick sedimentary sequences. *GSA Bull* 79:1097–1106.
- Carniglia SC (1986) Construction of the tortuosity factor from porosimetry. *J Catal* 102:401–418. [https://doi.org/10.1016/0021-9517\(86\)90176-4](https://doi.org/10.1016/0021-9517(86)90176-4).
- Clarkson CR, Bustin RM (1996) Variation in micropore capacity and size distribution with composition in bituminous coal of the Western Canadian Sedimentary Basin. *Fuel* 75:1483–1498. [https://doi.org/10.1016/0016-2361\(96\)00142-1](https://doi.org/10.1016/0016-2361(96)00142-1).
- Dullien FAL (1992) Porous media: fluid transport and pore structure, 2nd edn. Acad Press, San Diego, p 574.
- Expedition 337 Scientists (2013) Site C0020. In: Inagaki F, Hinrichs K-U, Kubo Y, the Expedition 337 Scientists (eds) Proc. IODP, 337. Integrated Ocean Drilling Program Management International, Inc., Tokyo. <https://doi.org/10.2204/iodp.proc.337.103.2013>.
- Fernández Pinto VE, Vaamonde G, Montani ML (1991) Influence of water activity, temperature and incubation time on the accumulation of aflatoxin B1 in soybeans. *Food Microbiol* 8:195–201. [https://doi.org/10.1016/0740-0020\(91\)90050-C](https://doi.org/10.1016/0740-0020(91)90050-C).
- Filomena CM, Stollhofen H, van Ojik K (2012) High-resolution ultrasonic measurements as proxies to resolve clastic reservoir heterogeneity in a salt-cemented gas reservoir/Geohorizon. *Am Assoc Pet Geol Bull* 96:1197–1209.
- Fredrickson JK, McKinley JP, Bjornstad BN, Long PE, Ringelberg DB, White DC, Krumholz LR, Suflita JM, Colwell FS, Lehman RM, Phelps TJ, Onstott TC (1997) Pore-size constraints on the activity and survival of subsurface bacteria in a late cretaceous shale-sandstone sequence, northwestern New Mexico. *Geomicrobiol J* 14:183–202. <https://doi.org/10.1080/01490459709378043>.
- Gamson PD, Beamish BB, Johnson DP (1993) Coal microstructure and microporosity and their effects on natural gas recovery. *Fuel* 72:87–99. [https://doi.org/10.1016/0016-2361\(93\)90381-B](https://doi.org/10.1016/0016-2361(93)90381-B).
- Glombitza C, Adhikari RR, Riedinger N, Gilhooly WP, Hinrichs K-U, Inagaki F (2016) Microbial sulfate reduction potential in coal-bearing sediments down to ~2.5 km below the seafloor off Shimokita peninsula, Japan. *Front Microbiol* 7:1576. <https://doi.org/10.3389/fmicb.2016.01576>.
- Grant WD (2004) Life at low water activity. *Philos Trans R Soc London Ser B Biol Sci* 359:1249–1267. <https://doi.org/10.1098/rstb.2004.1502>.
- Griffin DM (1972) Ecology of soil fungi. Chapman and Hall, London.
- Gross D, Bechtel A, Harrington GJ (2015) Variability in coal facies as reflected by organic petrological and geochemical data in Cenozoic coal beds offshore Shimokita (Japan)—IODP Exp. 337. *Int J Coal Geol* 152:63–79. <https://doi.org/10.1016/j.coal.2015.10.007>.
- Hinrichs K-U, Inagaki F (2012) Downsizing the deep biosphere. *Science* (80-) 338:204–205. <https://doi.org/10.1126/science.1229296>.
- Hoehler TM, Jørgensen BB (2013) Microbial life under extreme energy limitation. *Nat Rev Microbiol* 11:83–94. <https://doi.org/10.1038/nrmicro2939>.
- Huettel M, Gust G (1992) Impact of bioroughness on interfacial solute exchange in permeable sediments. *Mar Ecol Prog Ser* 89:253–267.
- Hunt JM, Whelan JK, Eglinton LB, Cathles LMI (1994) Gas generation—a major cause of deep Gulf Coast overpressure. *Oil Gas J* 92:59–63.
- Hunt JM, Whelan JK, Eglinton LB, Lii LMC (1998) Relation of shale porosities, gas generation, and compaction to deep overpressures in the U.S. Gulf Coast. In: Law BE, Ulmishek GF, Slavov VI (eds) Abnormal pressures in hydrocarbon environments. AAPG, Tulsa, pp 87–104.
- Ijiri A, Ikegawa Y, Inagaki F (2017) Data report: permeability of ~1.9 km-deep coal-bearing formation samples off the Shimokita Peninsula, Japan. In: Inagaki F, Hinrichs K-U, Kubo Y, the Expedition 337 Scientists (eds) Proceedings of the Integrated Ocean Drilling Program, 337. Integrated Ocean Drilling Program Management International, Inc., Tokyo. <https://doi.org/10.2204/iodp.proc.337.202.2017>.
- Inagaki F, Hinrichs K-U, Kubo Y, Bowles MW, Heuer VB, Hong W-L, Hoshino T, Ijiri A, Imachi H, Ito M, Kaneko M, Lever MA, Lin Y-S, Methe BA, Morita S, Morono Y, Tanikawa W, Bihan M, Bowden SA, Elvert M, Glombitza C, Gross D, Harrington GJ, Hori T, Li K, Limmer D, Liu C-H, Murayama M, Ohkouchi N, Ono S, Park Y-S, Phillips SC, Prieto-Mollar X, Purkey M, Riedinger N, Sanada Y, Sauvage J, Snyder G, Susilawati R, Takano Y, Tasumi E, Terada T, Tomaru H, Trembath-Reichert E, Wang DT, Yamada Y (2015) Exploring deep microbial life in coal-bearing sediment down to 2.5 km below the ocean floor. *Science* (80-) 349:420–424. <https://doi.org/10.1126/science.aaa6882>.
- Inagaki F, Hinrichs KU, Kubo Y, the Expedition 337 Scientists (2012) Deep coalbed biosphere off Shimokita: microbial processes and hydrocarbon system associated with deeply buried coalbed in the ocean. In: IODP Prel. Rept., 337. <https://doi.org/10.2204/iodp.pr.337.2012>.
- Inagaki F, Suzuki M, Takai K, Oida H, Sakamoto T, Aoki K, Nealson KH, Horikoshi K (2004) Microbial communities associated with geological horizons in coastal subseafloor sediments from the Sea of Okhotsk. *Appl Environ Microbiol* 69:7224–7235. <https://doi.org/10.1128/AEM.69.12.7224-7235.2003>.
- Jenkins MB, Bowman DD, Fogarty EA, Ghiore WC (2002) *Cryptosporidium parvum* oocyst inactivation in three soil types at various temperatures and water potentials. *Soil Biol Biochem* 34:1101–1109. [https://doi.org/10.1016/S0038-0717\(02\)00046-9](https://doi.org/10.1016/S0038-0717(02)00046-9).
- Jørgensen BB (2000) Bacteria and marine biogeochemistry. In: Schulz HD, Zabel M (eds) Marine Geochemistry. Springer Berlin Heidelberg, Berlin, Heidelberg, pp 173–207.
- Kallmeyer J, Pockalny R, Adhikari RR, Smith DC, D'Hondt S (2012) Global distribution of microbial abundance and biomass in subseafloor sediment. *Proc Natl Acad Sci* 109:16213–16216. <https://doi.org/10.1073/pnas.1203849109>.

- Laubach SE, Marrett RA, Olson JE, Scott AR (1998) Characteristics and origins of coal cleat: a review. *Int J Coal Geol* 35:175–207. [https://doi.org/10.1016/S0166-5162\(97\)00012-8](https://doi.org/10.1016/S0166-5162(97)00012-8).
- Lavelle P, Spain AV (2001) Soil ecology. Kluwer Academic Publishers, Dordrecht.
- Law BE (1984) Relationships of source-rock, thermal maturity, and overpressuring to gas generation and occurrence in low-permeability Upper Cretaceous and lower Tertiary rocks, Greater Green River basin, Wyoming, Colorado, and Utah, pp 469–490.
- León y León CA (1998) New perspectives in mercury porosimetry. *Adv Colloid Interf Sci* 76–77:341–372 doi: [https://doi.org/10.1016/S0001-8686\(98\)00052-9](https://doi.org/10.1016/S0001-8686(98)00052-9).
- Lever MA, Rogers KL, Lloyd KG, Overmann J, Schink B, Thauer RK, Hoehler TM, Jørgensen BB (2015) Life under extreme energy limitation: a synthesis of laboratory- and field-based investigations. *FEMS Microbiol Rev* 39:688–728 doi: doi.org/10.1093/femsre/fuv020.
- Lipp JS, Morono Y, Inagaki F, Hinrichs K-U (2008) Significant contribution of Archaea to extant biomass in marine subsurface sediments. *Nature* 454:991–994.
- Liu C-H, Huang X, Xie T-N, Duan N, Xue Y-R, Zhao T-X, Lever MA, Hinrichs K-U, Inagaki F (2017) Exploration of cultivable fungal communities in deep coal-bearing sediments from ~1.3 to 2.5 km below the ocean floor. *Environ Microbiol* 19:803–818. <https://doi.org/10.1111/1462-2920.13653>.
- Masui N, Morono Y, Inagaki F (2008) Microbiological assessment of circulation mud fluids during the first operation of riser drilling by the deep-earth research vessel *Chikyu*. *Geomicrobiol J* 25:274–282. <https://doi.org/10.1080/01490450802258154>.
- Morono Y, Terada T, Masui N, Inagaki F (2009) Discriminative detection and enumeration of microbial life in marine subsurface sediments. *ISME J* 3:503–511.
- Musslewhite CL, McInerney MJ, Dong H, Onstott TC, Green-Blum M, Swift D, Macnaughton S, White DC, Murray C, Chien Y-J (2003) The factors controlling microbial distribution and activity in the shallow subsurface. *Geomicrobiol J* 20:245–261. <https://doi.org/10.1080/01490450303877>.
- Osawa M, Nakanishi S, Tanahashi M, Oda H (2002) Structure, tectonic evolution and gas exploration potential of offshore Sanriku and Hidaka provinces, Pacific Ocean, off northern Honshu and Hokkaido, JAPAN. *J Japanese Assoc Pet Technol* 67:38–51. https://doi.org/10.3720/japt.67.1_38.
- Osborne M, Swarbrick R (1997) Mechanisms for generating overpressure in sedimentary basins: a reevaluation. *AAPG Bull* 81:1023–1041.
- Osterman G, Keating K, Binley A, Slater L (2016) A laboratory study to estimate pore geometric parameters of sandstones using complex conductivity and nuclear magnetic resonance for permeability prediction. *Water Resour Res* 52:4321–4337. <https://doi.org/10.1002/2015WR018472>.
- Parkes RJ, Cragg BA, Bale SJ, Getliff JM, Goodman K, Rochelle PA, Fry JC, Weightman AJ, Harvey SM (1994) Deep bacterial biosphere in Pacific Ocean sediments. *Nature* 371:410–413.
- Parkes RJ, Cragg BA, Wellsbury P (2000) Recent studies on bacterial populations and processes in subsurface sediments: a review. *Hydrogeol J* 8:11–28. <https://doi.org/10.1007/PL00010971>.
- Phadnis HS, Santamarina JC (2011) Bacteria in sediments: pore size effects. *Géotechnique Lett* 1:91–93. <https://doi.org/10.1680/geolett.11.00008>.
- Phepels TJ, Pfiffner SM, Sargent KA, White DC (1994) Factors influencing the abundance and metabolic capacities of microorganisms in eastern coastal plain sediments. *Microb Ecol* 28:351–364. <https://doi.org/10.1007/BF00662028>.
- Prasad M (2003) Velocity-permeability relations within hydraulic units. *Geophysics* 68:108–117. <https://doi.org/10.1190/1.1543198>.
- Raiders RA, McInerney MJ, Revus DE, Torbati HM, Knapp RM, Jenneman GE (1986) Selectivity and depth of microbial plugging in Berea sandstone cores. *J Ind Microbiol* 1:195–203. <https://doi.org/10.1007/BF01569272>.
- Raven KG, Gale JE (1985) Water flow in a natural rock fracture as a function of stress and sample size. *Int J Rock Mech Min Sci Geomech Abstr* 22:251–261. [https://doi.org/10.1016/0148-9062\(85\)92952-3](https://doi.org/10.1016/0148-9062(85)92952-3).
- Rebata-Landa V, Santamarina JC (2006) Mechanical limits to microbial activity in deep sediments. *Geochem Geophys Geosyst* 7(11):n/a. <https://doi.org/10.1029/2006GC001355>, <https://agupubs.onlinelibrary.wiley.com/doi/full/10.1029/2006GC001355>.
- Schulz HN, Jørgensen BB (2001) Big Bacteria. *Annu Rev Microbiol* 55:105–137. <https://doi.org/10.1146/annurev.micro.55.1.105>.
- Scott AR (2002) Hydrogeologic factors affecting gas content distribution in coal beds. *Int J Coal Geol* 50:363–387 doi: [https://doi.org/10.1016/S0166-5162\(02\)00135-0](https://doi.org/10.1016/S0166-5162(02)00135-0).
- Stevenson A, Cray JA, Williams JP, Santos R, Sahay R, Neuenkirchen N, McClure CD, Grant IR, Houghton JDR, Quinn JP, Timson DJ, Patil SV, Singhal RS, Anton J, Dijksterhuis J, Hocking AD, Lievens B, Rangel DEN, Voytek MA, Gunde-Cimerman N, Oren A, Timmis KN, McGenity TJ, Hallsworth JE (2015) Is there a common water-activity limit for the three domains of life? *ISME J* 9:1333–1351.
- Štrajpoč D, Mastalerz M, Dawson K, Macalady J, Callaghan AV, Wawrik B, Turich C, Ashby M (2011) Biogeochemistry of microbial coal-bed methane. *Annu Rev Earth Planet Sci* 39:617–656. <https://doi.org/10.1146/annurev-earth-040610-133343>.
- Su X, Zhang L, Zhang R (2003) The abnormal pressure regime of the Pennsylvanian no. 8 coalbed methane reservoir in Liulin–Wupu District, Eastern Ordos Basin, China. *Int J Coal Geol* 53:227–239 doi: [https://doi.org/10.1016/S0166-5162\(03\)00015-6](https://doi.org/10.1016/S0166-5162(03)00015-6).
- Sutherland JP, Bayliss AJ, Roberts TA (1994) Predictive modelling of growth of *Staphylococcus aureus*: the effects of temperature, pH and sodium chloride. *Int J Food Microbiol* 21:217–236. [https://doi.org/10.1016/0168-1605\(94\)90029-9](https://doi.org/10.1016/0168-1605(94)90029-9).
- Swarbrick R, Osborne M (1998) Mechanisms that generate abnormal pressures: an overview. In: Law BE, Ulmishek GF, Slavin VI (eds) *Abnormal pressures in hydrocarbon environments*. AAPG, Tulsa, pp 13–34.
- Takano O, Itoh Y, Kusumoto S (2013) Variation in forearc basin configuration and basin-filling depositional systems as a function of trench slope break development and strike-slip movement: examples from the Cenozoic Ishikari–Sanriku–Oki and Tokai–Oki–Kumano–Nada forearc basins, Japan. In: APM (ed) Itoh YBT-M of SBF-MA. InTech, Rijeka, p 11.
- Tanikawa W, Hirose T, Mukoyoshi H, Tadao O, Lin W (2013) Fluid transport properties in sediments and their role in large slip near the surface of the plate boundary fault in the Japan Trench. *Earth Planet Sci Lett* 382:150–160. <https://doi.org/10.1016/j.epsl.2013.08.052>.
- Tanikawa W, Ohtomo Y, Snyder G, Morono Y, Kubo Y, Iijima Y, Noguchi T, Hinrichs KU, Inagaki F (2018) Data report: water activity of the deep coal-bearing basin off Shimokita from IODP Expedition 337. In: Inagaki F, Hinrichs K-U, Kubo Y, the Expedition 337 Scientists (eds) *Proceedings of the Integrated Ocean Drilling Program, 337*. IODP-Management International, Inc., Tokyo. <https://doi.org/10.2204/iodp.proc.337.204.2018>.
- Tanikawa W, Tadao O, Morita S, Lin W, Yamada Y, Sanada Y, Moe K, Kubo Y, Inagaki F (2016) Thermal properties and thermal structure in the deep-water coalbed basin off the Shimokita Peninsula, Japan. *Mar Pet Geol* 73:445–461. <https://doi.org/10.1016/j.marpetgeo.2016.03.006>.
- Taylor SW, Millly PCD, Jaffé PR (1990) Biofilm growth and the related changes in the physical properties of a porous medium: 2. Permeability. *Water Resour Res* 26:2161–2169. <https://doi.org/10.1029/WR026i009p02161>.
- Tomaru H, Fehn U, Lu Z, Takeuchi R, Inagaki F, Imachi H, Kotani R, Matsumoto R, Aoike K (2009) Dating of dissolved iodine in pore waters from the gas hydrate occurrence offshore Shimokita peninsula, Japan: ¹²⁹I results from the *CV Chikyu* shakedown cruise. *Resour Geol* 59:359–373. <https://doi.org/10.1111/j.1751-3928.2009.00103.x>.
- Trembath-Reichert E, Morono Y, Ijiri A, Hoshino T, Dawson KS, Inagaki F, Orphan VJ (2017) Methyl-compound use and slow growth characterize microbial life in 2-km-deep subsurface coal and shale beds. *Proc Natl Acad Sci* 114:E9206 LP–E92E9215.
- Updegraff DM (1983) Plugging and penetration of petroleum reservoir rock by microorganisms. In: *Proceedings of the 1982 International Conference on Microbial Enhancement of Oil Recovery*. Shangri-La, Afton, Oklahoma. B. Linville. Bartlesville Energy Technology Center, Bartlesville, p 85.
- Vandevivere P, Baveye P, de Lozada DS, DeLeo P (1995) Microbial clogging of saturated soils and aquifer materials: evaluation of mathematical models. *Water Resour Res* 31:2173–2180. <https://doi.org/10.1029/95WR01568>.
- Wangen M (1997) Two-phase oil migration in compacting sedimentary basins modelled by the finite element method. *Int J Numer Anal Methods Geomech* 21:91–120. [https://doi.org/10.1002/\(SICI\)1096-9853\(199702\)21:2<91::AID-NAG860>3.0.CO;2-L](https://doi.org/10.1002/(SICI)1096-9853(199702)21:2<91::AID-NAG860>3.0.CO;2-L).
- Wibberley CAJ (2002) Hydraulic diffusivity of fault gouge zones and implications for thermal pressurization during seismic slip. *Earth Planets Space* 54(11): 1153–1171 doi: doi.org/10.1186/BF03353317.
- Williams JP, Hallsworth JE (2009) Limits of life in hostile environments: no barriers to biosphere function? *Environ Microbiol* 11:3292–3308. <https://doi.org/10.1111/j.1462-2920.2009.02079.x>.
- Witherspoon PA, Wang JSY, Iwai K, Gale JE (1980) Validity of cubic law for fluid flow in a deformable rock fracture. *Water Resour Res* 16:1016–1024. <https://doi.org/10.1029/WR016i006p01016>.
- Yakimov MM, Amro MM, Bock M, Boseker K, Fredrickson HL, Kessel DG, Timmis KN (1997) The potential of *Bacillus* licheniformis strains for in situ enhanced

oil recovery. *J Pet Sci Eng* 18:147–160 doi: [https://doi.org/10.1016/S0920-4105\(97\)00015-6](https://doi.org/10.1016/S0920-4105(97)00015-6).

Zhang C, Palumbo AV, Phelps TJ, Beauchamp JJ, Brockman FJ, Murray CJ, Parsons BS, Swift DJP (1998) Grain size and depth constraints on microbial variability in coastal plain subsurface sediments. *Geomicrobiol J* 15:171–185. <https://doi.org/10.1080/01490459809378074>.

Zhao J, Li J, Xu Z (2018) Advances in the origin of overpressures in sedimentary basins. *Pet Res* 3:1–24. <https://doi.org/10.1016/j.ptlrs.2018.03.007>.

Submit your manuscript to a SpringerOpen[®] journal and benefit from:

- ▶ Convenient online submission
- ▶ Rigorous peer review
- ▶ Open access: articles freely available online
- ▶ High visibility within the field
- ▶ Retaining the copyright to your article

Submit your next manuscript at ▶ [springeropen.com](https://www.springeropen.com)
